

Simulation of Molten Corium Concrete Interaction in a Stratified Configuration: the COMET-L2-L3 Benchmark

B. Spindler¹, K. Atkhen², M. Cranga³, J. Foit⁴,
M. Garcia⁵, W. Schmidt⁶, T. Sevon⁷, C. Spengler⁸

- | | |
|----------------------------------|-------------------------|
| 1) CEA/DEN, Grenoble (FR) | 5) UPM, Madrid (E) |
| 2) EDF/SEPTEN, Villeurbanne (FR) | 6) AREVA, Erlangen (DE) |
| 3) IRSN, Cadarache (FR) | 7) VTT, Espoo (Fin) |
| 4) FZK, Karlsruhe (DE) | 8) GRS, Cologne (DE) |

Summary

In the late phase of Molten Core Concrete Interaction (MCCI) the ablation rate becomes low and the gas flow rate issued from the concrete decomposition is reduced. Moreover the oxide phase becomes lighter than the metal phase due to the addition of the light oxide from the concrete. A large density difference and a low gas flow rate ensure that a stratified configuration will occur. The stratified configuration has then to be taken into account in the MCCI simulation tools. Only few experimental programs were conducted with stratified pools; among them the BETA tests were performed at FZK with a large test matrix. The COMET-L2 and L3 experiments were recently conducted at FZK in a stratified configuration. In the frame of SARNET WP11.2 a benchmark was organised in order to compare the MCCI code results regarding these experiments. COMET-L2 was used for a post-test simulation and after that COMET-L3 was used as a blind simulation. The participants and codes were AREVA with COSACO, CEA with TOLBIAC-ICB, EDF with TOLBIAC-ICB, FZK with WECHSL, GRS with MEDICIS and WEX, IRSN with MEDICIS, UPM with MELCOR and VTT with MELCOR. The results show a large discrepancy between the code results, due to the different models used in the stratified regime.

A. INTRODUCTION

In the event of a severe accident in a Pressurized Water Reactor, corium, a mixture of molten materials issued from the fuel, cladding and structural elements, appears in the reactor core. In some scenarios, corium is assumed to melt through the reactor pressure vessel and spread over the concrete basemat of the reactor pit. Molten Core Concrete Interaction (MCCI) then occurs, characterized by concrete ablation. The main question that has to be addressed is whether and when the corium will make its way through the basemat since it would lead to a failure of the containment. The MCCI phenomena occurring in case of an oxide corium pool have been largely investigated and uncertainties are still not resolved, concerning for instance the lateral and axial ablation rates (Ref [1]).

In the late phase of MCCI the ablation rate becomes low and the gas flow rates from the decomposing concrete are reduced. Moreover the oxide phase becomes lighter than the metal phase due to the addition of the light oxide from the concrete. A large density difference and a low gas flow rate ensure that a stratified configuration will occur. The stratified configuration has then to be taken into consideration and has to be modelled in the MCCI simulation tools.

After a description of the facility and of the COMET-L2 and COMET-L3 tests, the results of the benchmarks are presented. A short description of the codes used, with emphasis on the model used in the stratified configuration is then given.

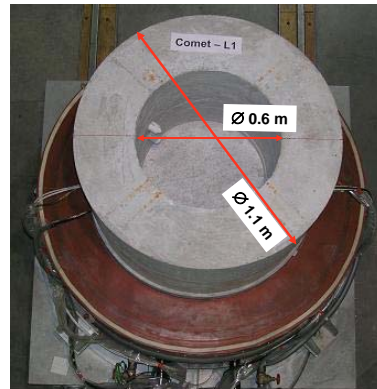
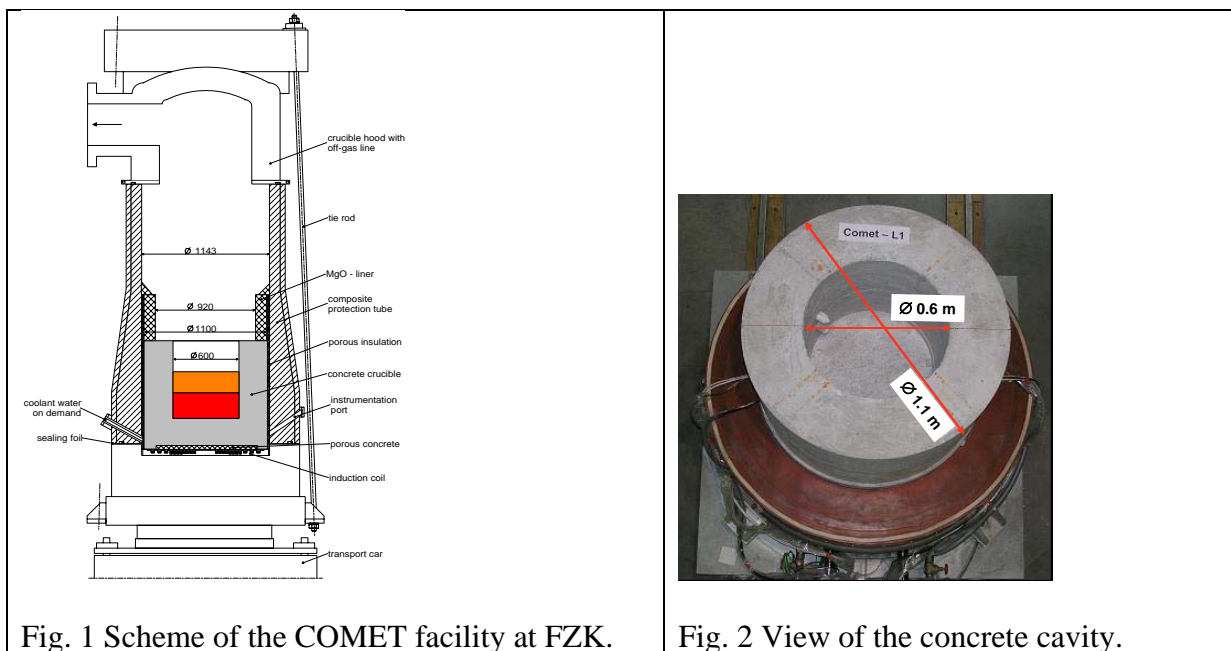
B. COMET-L2 AND L3 EXPERIMENTS

B1. The experimental facility

The COMET-L2 and L3 tests were performed at the Forschungszentrum Karlsruhe (FZK). Only the main characteristics of the facility and of the tests are given here. More details are given of the report from FZK (Ref [2] and [3]).

A cylindrical siliceous concrete cavity of 0.6 m diameter is supported by a device including the induction heating coil at the bottom (Fig. 1-2). The simulated corium melt is generated externally by an alumina thermite reaction and poured into the crucible through a lid in the upper hood. This moment defines the experimental time zero, when the dry erosion starts. When the melt approaches the light guides at the bottom of the crucible, the test will stop and flooding is initiated in order to prevent damage of the facility. During the course of the test, continuous heating takes place through the induction coil. The heavy metal phase heated by induction is overlaid by the light oxide phase in which no sustained heating is provided.

The outer crucible is gas tight, so all gases generated during the experiment are collected in the free volume of the crucible and feed through the off-gas system into the ambient atmosphere. A constant argon cover gas flow is injected into the crucible to prevent the accumulation of a burnable gas mixture. In the off-gas system, the main characteristics such as temperature, composition and flow rate of the released gases are measured online.



The COMET facility is equipped with a multitude of instrumentation to monitor and control the experiment and to collect the data for subsequent evaluation. The ablation evolution is deduced from the signal of thermocouples embedded in the concrete crucible. The thermocouples are of type NiCr-Ni. They fail at about 1620 K, and therefore they operate until melting of the concrete does occur. Their failure indicates arrival of the melt front. They are unable to measure the temperature of the melt. Fig 3 gives for instance the position of the thermocouples in the SW-NE plane for COMET-L3.

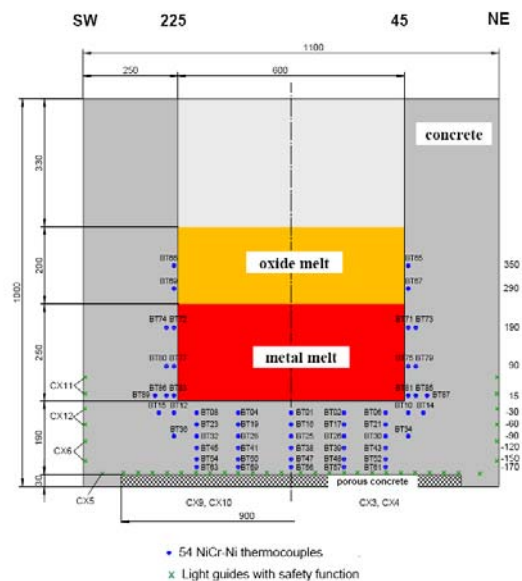


Fig. 3 Thermocouples and light guides instrumentation in the plane NW-SE of COMET-L3 test section.

B2. COMET-L2

The COMET-L2 test was performed in the frame of the LACOMERA project of the 5th European Framework Programme, with participation of ARC Seibersdorf (Austria). It was conducted on February 5, 2005.

The initial composition of the melt was 430 kg metal with 90 % iron and 10 % nickel and 35 kg oxide with 56 % alumina and 44 % calcia. The mean heating power was 200 kW and the initial temperature was 2023 K. The heating power was switched off automatically at 1015 s, by failure of a light guide. The bottom flooding of the crucible started at 1440 s.

After an initial period of about 100 s until end of overheat, characterized by an isotropic ablation, a steady state regime is reached, with a faster axial ablation compared to the lateral ablation (factor 2 to 3), which is in agreement with the results of the BETA experiments at low power density. A view of the final shape of the cavity is presented on figure 4.

B3. COMET-L3

The COMET-L3 was conducted on November 12, 2005.

The initial composition of the melt was 425 kg metal with 90 % iron and 10 % nickel and 211 kg oxide with 56 % alumina and 44 % calcia. The mean heating power was 220 kW and the initial temperature was 1940 K. Top flooding was initiated by shower at 800 s. The heating power was switched off automatically at 1878 s, by failure of a light guide.

After an initial period of about 100 s until end of overheat, characterized by an isotropic ablation, a steady state regime is reached, with a faster axial ablation compared to the lateral ablation (factor 2 to 3), which is in agreement with the results of the COMET-L2 experiment. Flooding does not lead to strong melt-water interaction, and the concrete ablation is a little reduced. A view of the final shape of the cavity is presented on figure 5.

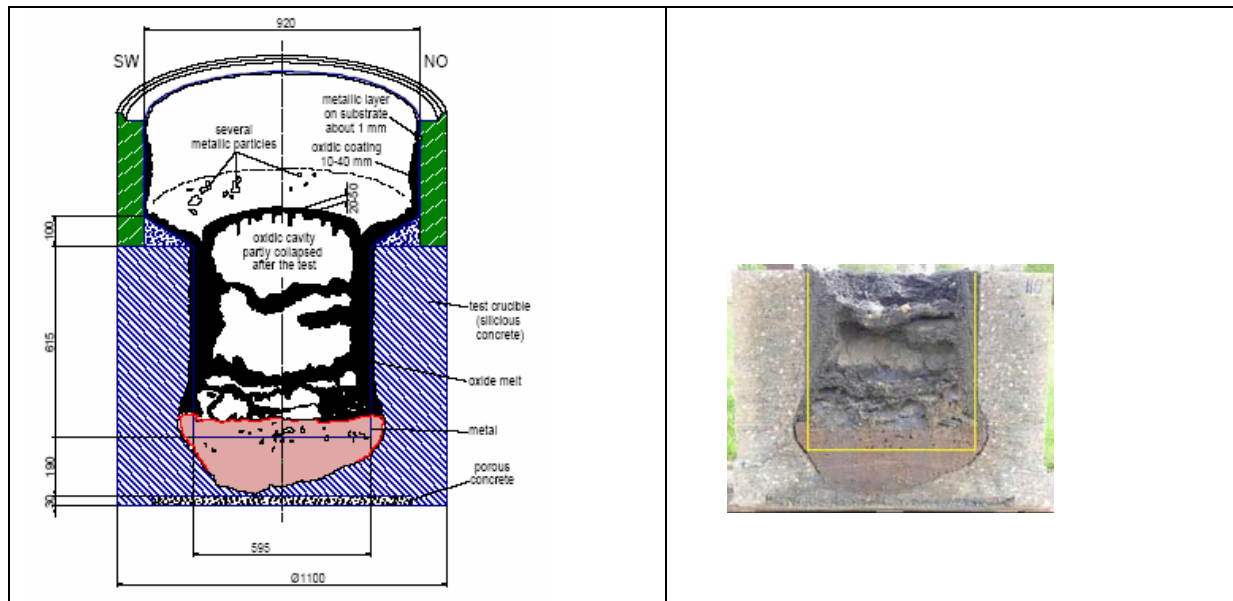


Fig. 4 COMET-L2: view of the concrete crucible sectioned in direction SW-NE.

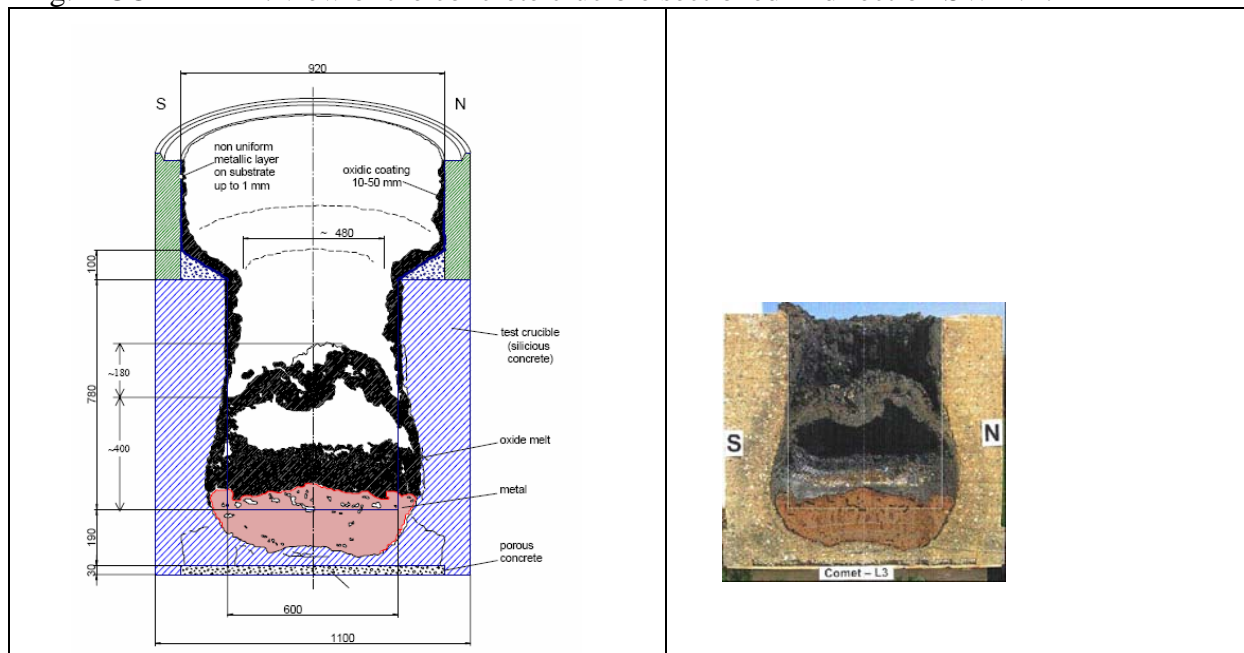


Fig. 5 COMET-L3: view of the concrete crucible sectioned to plane S-N.

C. RESULTS OF THE COMET-L2 BENCHMARK

The COMET-L2 test was used for a post test benchmark. The data given to the code users were the geometry of the cavity, the concrete composition and physical properties, the melt initial composition and temperature, the input power evolution versus time, and the data useful for the radiation model (emissivity and surroundings temperature). The participants were AREVA with COSACO, CEA with TOLBIAC-ICB, EDF with TOLBIAC-ICB, FZK with WECHSL, GRS with MEDICIS and with WEX, IRSN with MEDICIS and VTT with MELCOR. CEA and IRSN presented a base calculation and calculations with some modifications of the models in order to get a better agreement with the experimental results. The corresponding results are quoted with “mod” in the figures. The results are presented on figures 6 to 11.

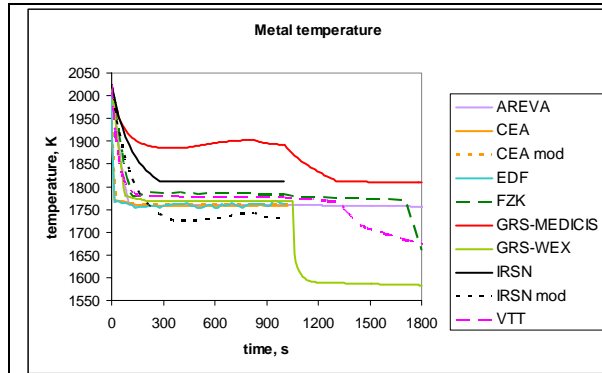


Fig. 6 COMET-L2: calculated metal temperature versus time.

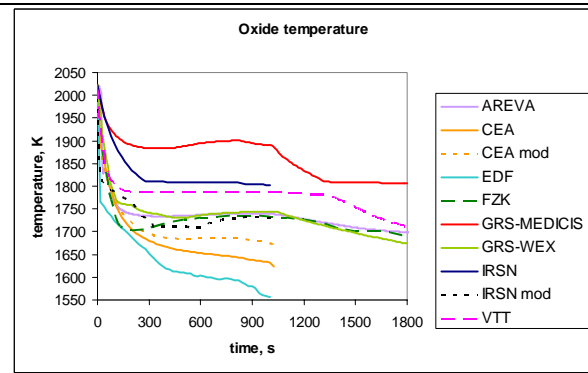


Fig. 7 COMET-L2: calculated oxide temperature versus time.

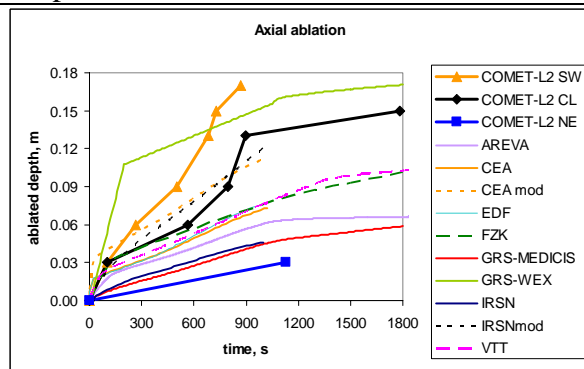


Fig. 8 COMET-L2: calculated and measured axial ablation versus time.

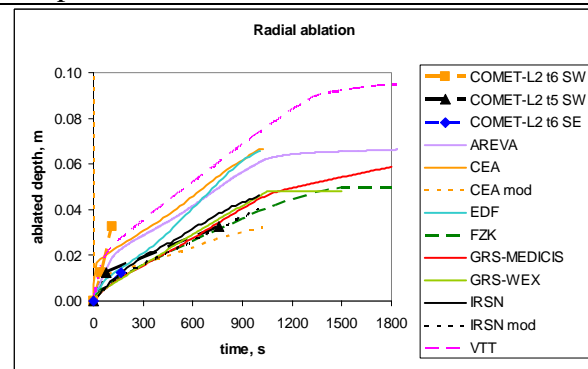


Fig. 9 COMET-L2: calculated and measured lateral ablation versus time.

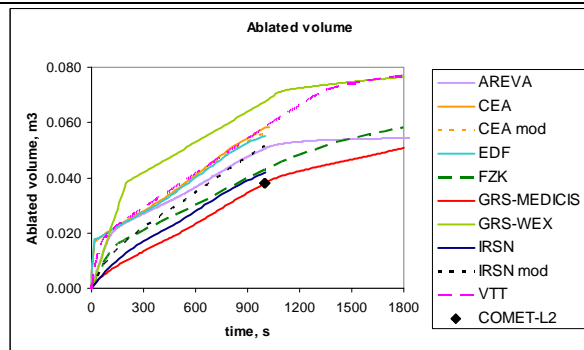


Fig. 10 COMET-L2: calculated ablated volume versus time and final experimental value.

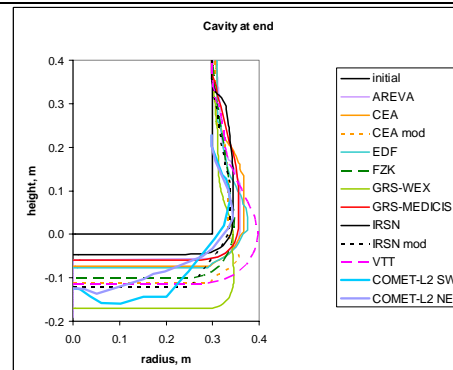


Fig. 11 COMET-L2: final calculated and measured shape of the cavity.

Some calculations were stopped at the time the heating power is switched off (1015 s) while others continue until 1800 s. The first rapid temperature decrease corresponds to the initial overheating of the melt until a steady state regime is reached. It corresponds to a high ablation rate. After that the ablation rate is reduced; it remains rather constant and the metal temperature is quite constant while for some codes the oxide temperature continuously decreases. The scatter between the calculated metal temperatures is about 150 K, but six results are between 1750 and 1780 K. The scatter between the oxide temperatures is larger: about 450 K at 1000 s.

There is also a large scatter concerning the ablation depth, but it can be noticed that after the first phase corresponding to the initial overheating, the ablation rate is similar for all the codes. Finally when compared to the experimental results, it is found that the maximum axial ablation is underestimated. It can be seen also that the modification of some models (mainly

the ratio of the axial to the radial heat transfer coefficients) made by CEA and IRSN leads to results closer to the experiments than the base case results.

D. RESULTS OF THE COMET-L3 BENCHMARK

The COMET-L3 test was used for a blind test benchmark: the experimental results were not known when the calculations were performed. The data given to the code users were the geometry of the cavity, the concrete composition and physical properties, the melt initial composition and temperature, the input power evolution versus time, and the data useful for the radiation model (emissivity and surroundings temperature). The participants were AREVA with COSACO, CEA with TOLBIAC-ICB, EDF with TOLBIAC-ICB, FZK with WECHSL, GRS with MEDICIS and with WEX, IRSN with MEDICIS, UPM with MELCOR and VTT with MELCOR. The results are presented on figures 12 to 25.

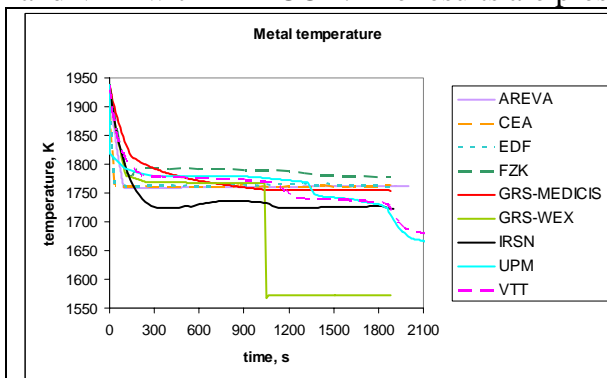


Fig. 12 COMET-L3: calculated metal temperature versus time.

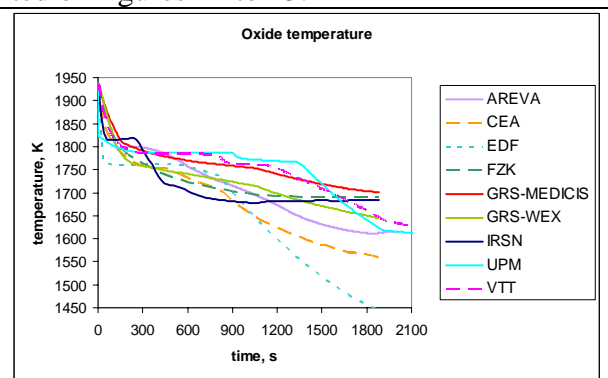


Fig. 13 COMET-L3: calculated oxide temperature versus time.

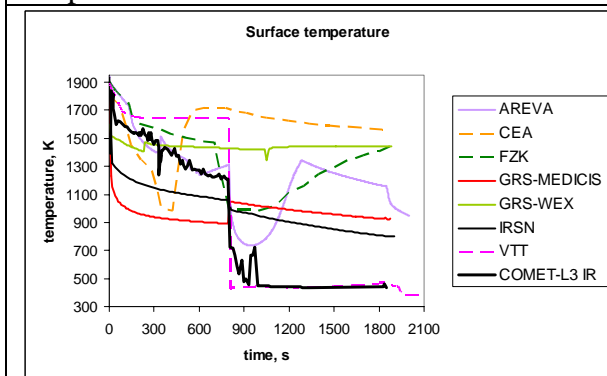


Fig. 14 COMET-L3: calculated top surface temperature versus time.

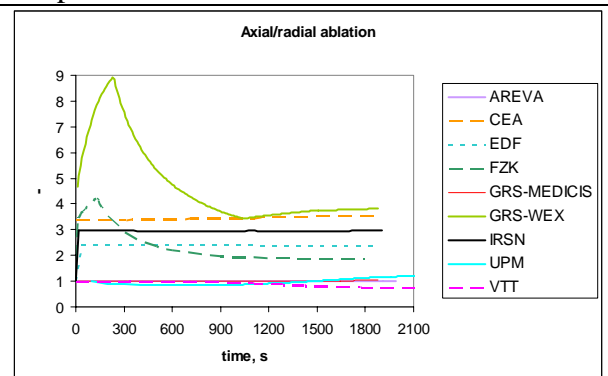


Fig. 15 COMET-L3: calculated axial to lateral ablation rate versus time.

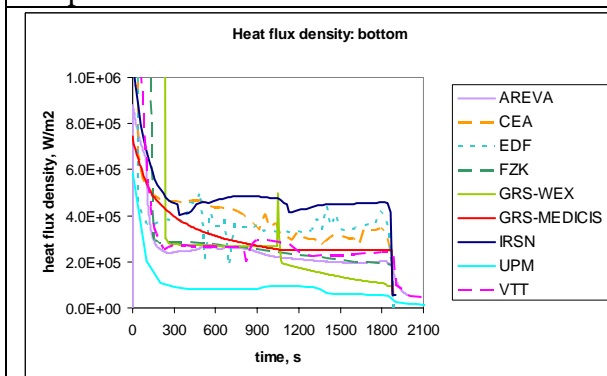


Fig. 16 COMET-L3: calculated bottom heat flux density versus time.

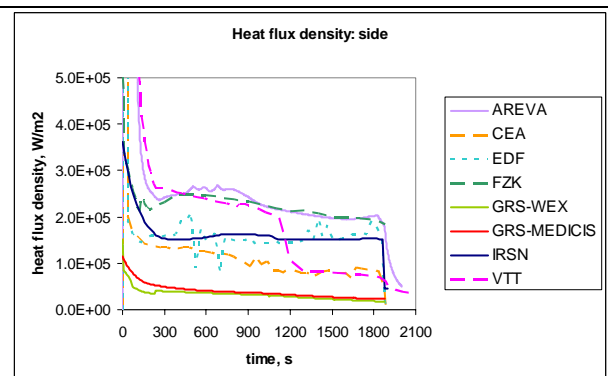


Fig. 17 COMET-L3: calculated metal lateral heat flux density versus time.

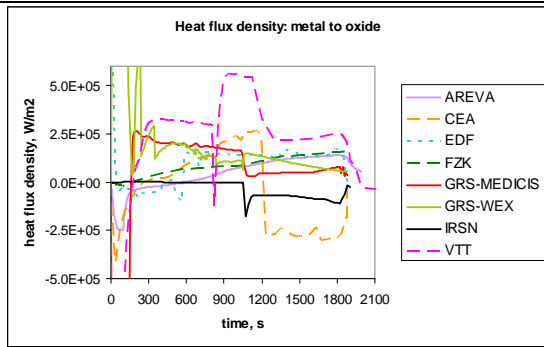


Fig. 18 COMET-L3: calculated metal to oxide heat flux density versus time.

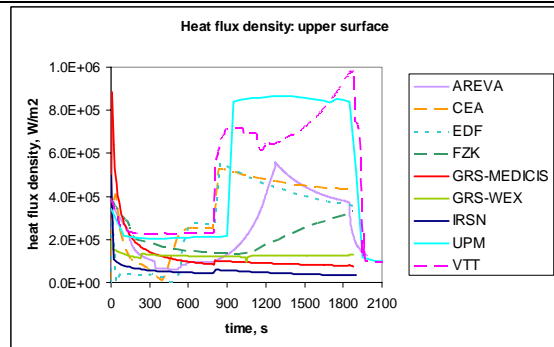


Fig. 19 COMET-L3: calculated top surface heat flux density versus time.

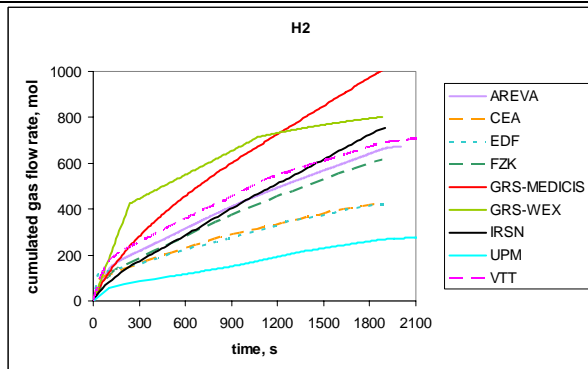


Fig. 20 COMET-L3: calculated hydrogen ejection versus time.

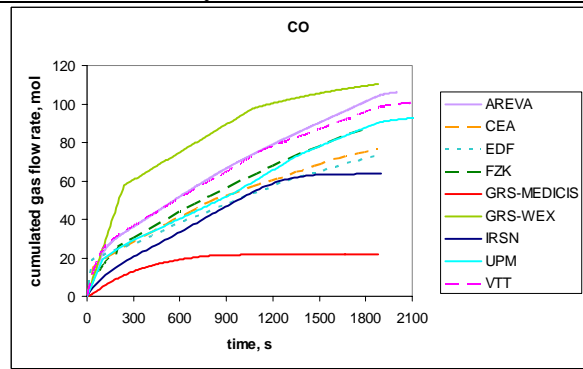


Fig. 21 COMET-L3: calculated carbon monoxide ejection versus time.

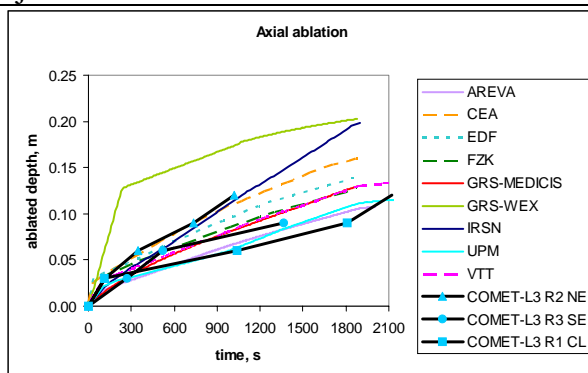


Fig. 22 COMET-L3: calculated and measured axial ablation versus time.

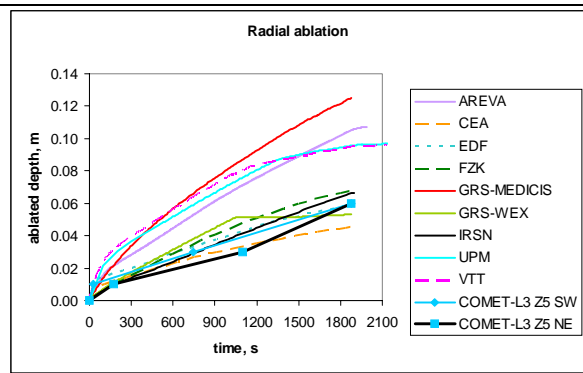


Fig. 23 COMET-L3: calculated and measured lateral ablation versus time.

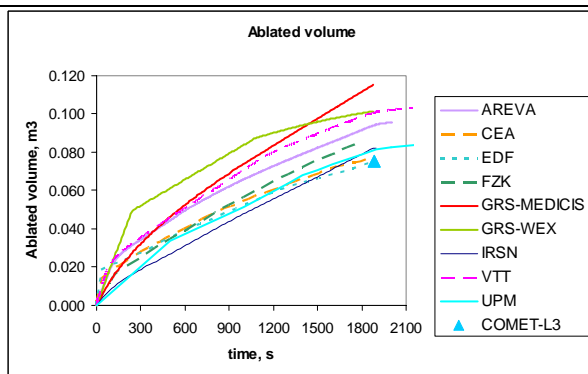


Fig. 24 COMET-L3: calculated ablated volume versus time and final experimental value.

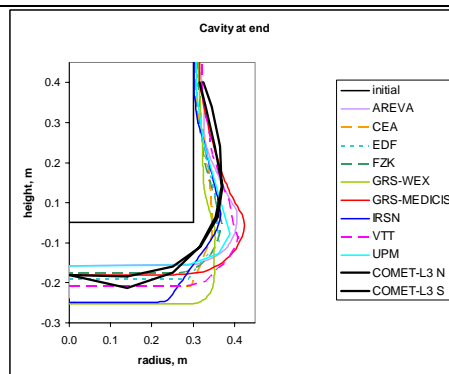


Fig. 25 COMET-L3: final calculated and measured shape of the cavity.

Some calculations were stopped at the time the heating power is switched off (1800 s) while others continue until 2100 s. As for COMET-L2 test, the first rapid temperature decrease corresponds to the initial overheat of the melt until a steady state regime is reached. It corresponds to a high ablation rate. After that the ablation rate is reduced; it remains rather constant even after top flooding at 800 s. The top flooding is sensitive for one calculated temperature only. It can be observed that the scatter of the calculated oxide and metal temperatures is reduced compared to COMET-L2 (Fig. 12 and 13).

Concerning the surface temperature (Fig. 14), the scatter is about 800 K before top flooding and 1300 K after. The experimental measurement is also given: it is located more or less in the middle of the code results before flooding. After flooding only one code gives the water temperature as top surface temperature.

Figure 15 shows the axial to lateral ablation rate versus time. It is fixed in most of the codes, either at 1, or at a value near 3, this value being chosen for a best prediction of the experiment. For two codes the ratio is varying with time.

The heat flux density from the metal layer to the bottom and the side concrete walls are also drawn on figures 16 and 17. After the initial phase, the ratio between the larger and the lower value is about 5. Also interesting is the heat flux density between the metal and the oxide layer (fig. 18). In the initial phase some codes give a heat transfer from the oxide to the metal (negative value) and the others from the metal to the oxide (positive value). In the second phase before flooding, all codes predict heat transfer from the metal to the oxide. After flooding some codes give back a heat transfer from the oxide to the metal. Figure 19 shows the evolution of the top surface heat flux density versus time. The effect of flooding leads to an increase of the heat flux density, more or less, except for three codes.

The gas issued from the concrete decomposition flows through the metal layer, giving some oxidation. It is interesting to look at the code prediction concerning gas production since it has consequences for the safety of the containment. Figure 20 gives the cumulated production of hydrogen and figure 21 the cumulated production of carbon monoxide versus time. Here again the scatter is large, with about a factor 5 between the larger and the lower values.

There is also a large scatter concerning the ablation depth, the ablated volume and the final shape of the cavity (fig. 22 to 25). Some codes give results which are similar to the experimental results. Some others overestimate the axial ablation or the lateral ablation, and the ablated volume.

The objective here is not to explain in detail the results of each code concerning the COMET-L2 and L3 simulation. However, a short presentation of each code is given now, in order to have a view of how they deal with a stratified configuration. A recent paper (Ref. [4]) gives more details on the codes and their validations.

E. CODE MODELS FOR STRATIFIED CONFIGURATIONS

E1. COSACO

The COSACO code is developed by AREVA (Ref. [5]). The oxidic melt is modelled to predominantly solidify and to deposit as a crust at the cold boundaries of the pool. Crust formation commences during the incipient phase of the MCCI after the melt temperature falls below the liquidus line of the mixture. On the other hand, the MCCI process exhibits a unique phenomenon which is the continuous mixing of the melt pool with relatively cold concrete decomposition products. As a result, solidification also takes place in the volume aside from crust formation at the boundaries of the melt pool. Correspondingly, solid phases are modelled to stay in the volume, where they increase the viscosity and thus lead to retarding

the heat transfer to the melt/crust interface. The real solution database COSCHEM is integrated into the modelling logic of COSACO employing the equilibrium solver CHEMAPP. The data stored in COSCHEM essentially bases on the real solution database TDBCR 99. Contrary to oxide melts, the heat transfer model developed for metallic melts bases on the assumption that not the melt itself but a slag layer formed at the melt/concrete interface limits heat removal from the melt pool.

The modelling of the melt pool configuration takes into account two situations. In the case of a stratified configuration, phases having an oxidic character either concentrate in an oxidic or in a slag layer, while the metallic phases accumulate in a metallic layer. These thermochemically immiscible layers are connected by mass and energy transfer. Alternatively, a mixed model was developed to study the consequences of postulated gas-induced mechanical mixing on the MCCI.

The heat flux distribution along the periphery of the molten pool is assumed to be isotropic for both, metallic and oxidic melts. Following this assumption, lateral and axial ablation rates are predicted to be equal. The rationale behind this assumption is based on physical observations from a number of MCCI experiments. Further support of the sideward heat transfer modeling comes from the BALI experiments which examine the heat transfer in gas-agitated liquid pools. These experiments, performed to analyze upward and downward power distribution, indicated that gas injection favors an isotropic heat flux distribution.

E2. MEDICIS

The MEDICIS code is developed by IRSN and included in the reactor accident system code ASTEC (Ref. [6]). The solidification temperature is evaluated using a parametrical model to take into account any value of the liquid/crust interface temperature between solidus and liquidus temperatures and any pool bulk molten fraction with a possible mushy zone. More precisely, the solidification temperature is the temperature of the boundary between the outer conductive zone and the inner convective zone. In the calculations with MEDICIS presented here, IRSN uses an interface temperature equal or close to the liquidus temperature, whereas GRS uses an interface temperature equal to the solidus temperature.

In each pool layer, the corium layer/concrete interface is described as a combination of a corium crust, if existing, and of a slag layer composed of concrete material. The heat transfer at the pool/concrete interface is evaluated by a thermal resistance model taking into account the convective heat transfer in the corium layer and conduction across the crust and the slag layer. The crust thickness at the corium/concrete interface in a given pool layer is evaluated, using a quasi-steady state assumption, from the heat flux continuity relations at the inner and outer crust interfaces. The Nusselt number is evaluated from empirical correlations valid for a liquid/solid wall interface crossed by a gas flow. The default correlation is that of deduced from the BALI experiments, and other correlations are available in MEDICIS. The heat transfer coefficient in the slag layer is a user's input parameter. Instead of this serial combination of thermal resistances (convection, crust, slag) used by IRSN, GRS applies a single correlation for effective heat transfer derived from averaged experimental results.

The heat transfer between two adjacent layers is described by a thermal resistance model taking into account heat convection within each layer on both sides of the interface and heat conduction in the crust possibly appearing in each layer at this interface. The convective heat transfer at the interface between layers is described by a convective heat transfer mechanism driven by the gas bubbling. The convective heat transfer coefficient in each layer is given by the same relation as for a liquid/solid interface, but the correlation for the Nusselt number is that proposed by Greene, valid for the heat transfer between two adjacent immiscible liquid

layers in presence of gas bubbling, which increases considerably heat transfer compared to that occurring at a liquid/solid interface.

E3. MELCOR

The MELCOR code is developed at Sandia National Laboratory (Ref [7]). The models and material properties are taken from the CORCON-Mod3 code (Ref. [8]). The heat flux between the interior of each layer and its interfaces (with another layer, with concrete, or with the water pool or atmosphere above the melt surface) is treated separately. Continuity of the heat flux determines the temperature of each interface. Some of the layer axial or radial surfaces may be covered with solid crust. The crust inner surfaces are fixed to the solidus temperature, and the concrete surface is fixed to the ablation temperature. Heat transfer from the melt takes place by bubble-enhanced convection with different correlations for the axial and radial heat transfers. For the heat transfer between the oxidic and metallic layer, the Greene's correlation is used. An additional heat transfer resistance is present at the melt-concrete interface because of the assumed thin layer of concrete slag. It is taken into account by a slag heat transfer coefficient. Further, if a crust is present at the interface, conduction through the crust is calculated as heat transfer resistance. The solidus and liquidus temperatures of the mixtures are calculated by assuming that they form ideal solutions. The solidus temperatures of core-concrete mixtures measured by Roche are significantly lower than those calculated by CORCON and MELCOR.

MELCOR calculates the heat transfer from the top surface by natural convection and radiation, or by boiling if there is a water pool. Direct radiation to surrounding surfaces cannot be calculated with MELCOR. In COMET-L3 simulation, MELCOR predicted film boiling at the surface. The heat transfer coefficient from the surface was artificially increased in the calculation by VTT, so that the surface temperature was equal to 100 °C after the flooding, because the heat flux was well below the critical heat flux and hence no film boiling at the surface is expected.

E4. TOLBIAC-ICB

The TOLBIAC-ICB code is developed by CEA in the frame of an agreement with EDF. (Ref. [9]). It is based on the phase segregation model. Due to the high liquidus temperature of oxide melts and despite the melting of concrete and the presence of gas issued from concrete decomposition, a solid crust is assumed to form at the concrete wall. The species that encrust are the most refractory species. A low crust growth, a high liquid diffusivity and a small diffusion boundary layer thickness are also assumed. With this view, the pool is only composed of liquid and consequently has a low viscosity. The interface temperature between the liquid pool and the solid crust is equal to the liquidus temperature corresponding to the current composition of the remaining liquid phase. The crust thickness is calculated using a steady state assumption. Physico-chemistry in TOLBIAC-ICB code is calculated with an intrinsic coupling to the GEMINI2 code, developed by THERMODATA.

Concerning the stratified melt, one assumes in the COMET-L2 and L3 simulations that the two liquids are bounded with their own crust and have their own physico-chemistry characteristics. Another modification of the basic model concerns the oxide phase where no input power is provided in the COMET-L2 and L3 experiment. Consequently the model has been adapted for this specific case, allowing an oxide temperature below the liquids temperature.

The code user may select the heat transfer correlations that are used. In the calculations presented here, CEA used the same heat transfer correlation (BALI correlation) for the different interfaces, including the interface between the two layers, with a multiplying factor

for the lateral heat transfer. EDF used the Greene correlation between the two layers and also a multiplying factor for the lateral heat transfer.

E5. WECHSL

The WECHSL code was developed at FZK (Ref. [10], [11], [12]). For the heat transfer from melt to concrete, a film model, a discrete bubble model or a transition boiling model is used, depending on the existing gas flow and on the inclination of the interface. As the melt is intensively stirred by the gases released during the concrete ablation process, the bulk of each layer of the melt is assumed to be isothermal with boundary layers at the interfaces. During cooldown of the melt crust formation is modelled, starting from the metal-concrete interface and from the upper melt surface which eventually leads to a fully frozen layer. Crusts are assumed to be permeable to gases. The solidus and liquidus temperatures of the metallic phase are calculated from the chromium-nickel-iron, zirconium-iron and silicon-iron phase diagrams. For the oxide phase the solidus and liquidus temperatures are determined either from a quasi-binary phase diagram or from a user input table. It is assumed that the solidus and liquidus temperatures of a dispersed melt are equal to the ones of the pure oxide melt. Both the crusts and the liquid melt have the same composition. The viscosities of the oxide melt below the liquidus temperature are assumed to follow the modified Pinkerton-Stevenson correlation.

E6. WEX

WEX is a modified version of the WECHSL code that is developed by GRS and is included in the reactor accident system code ASTEC (Ref. [13]). Similar models are included in WECHSL and WEX, but the empirical fitting of heat transfer model parameters is different in each code. Specifically, the original gas film model for the bottom interface of the pool between metal and concrete and the viscosity model for oxide melts are kept unmodified in WEX as described in Ref. [10] and Ref. [12], respectively, but the Nusselt relation in WECHSL accounting for the effect of viscosity increase in the boundary layer of oxide melts has been extended in WEX by introducing additional parameters. These parameters were fitted versus a selection of experiments, including BETA and ACE tests. Heat transfer between the molten layers is calculated in WEX (like in WECHSL) by a Nusselt correlation obtained on the basis of analytical work performed by Haberstroh and Reinders with an enhancement due to gas percolation as deduced from the experiments of Werle (see Ref. [10]).

F. CONCLUSIONS

The COMET-L2 and COMET-L3 MCCI tests in a stratified configuration were used respectively for a post-test benchmark and a blind benchmark. These tests correspond to the late phase of MCCI in a reactor case, with a metallic layer at the bottom. Eight European organisations participate, with six different codes. The results show a large scatter of the different variables (temperatures, heat flux, ablation depth, gas production) and of the effect of top flooding. This scatter includes the results of a code used by different organisation with different models.

One can conclude that the MCCI phenomena are still not well understood. Future works are needed in this field, both concerning experiments and models. A benchmark concerning reactor cases is proposed in the frame of SARNET. It should complete the results presented here, and give a more useful view of the code performances, since the aim of the codes is to simulate reactor accidents rather than specific experiments.

References

- [1] M.T. Farmer, S. Lomperski, D. Kilsdonk, R.W. Aeschlimann, S. Basu, A Summary of Findings from the Melt Coolability and Concrete Interaction (MCCI) Program, International Congress on Advances in Nuclear Power Plants, Nice, France, May 13-18, 2007.
- [2] G. Sdouz, R. Mayrhofer, H. Alsmeyer, T. Cron, B. Fluhrer, J. Foit, G. Messemer, A. Miassoedov, S. Schmidt-Stiefel, T. Wenz, The COMET-L2 Experiment on Long-Term MCCI with Steel Melt, Forschungszentrum Karlsruhe, Wissenschaftliche Berichte, FZKA 7214 (2006) and SAM-LACOMERA-D15 (2006).
- [3] H. Alsmeyer, T. Cron, B. Fluhrer, G. Messemer, A. Miassoedov, S. Schmidt-Stiefel, T. Wenz, The COMET-L3 Experiment on Long-Term Melt-Concrete Interaction and Cooling by Surface Flooding, Forschungszentrum Karlsruhe, Wissenschaftliche Berichte, FZKA 7244 (2007).
- [4] H.J. Allelein, M. Bürger, Considerations on Ex-Vessel Corium Behavior: Scenarios, MCCI and Coolability, Nuclear Engineering and Design, 236 (2006), 2220-2236.
- [5] M. Nie, M. Fischer, G. Lohnert, Advanced MCCI Modelling Based on Stringent Coupling of Thermal Hydraulics and Real Solution Thermochemistry in COSACO, Proceedings 10th International Conference on Nuclear Engineering, ICONE 10, Arlington, VA, April 2002.
- [6] M. Cranga, R. Fabianelli, F. Jacq, M. Barrachin, F. Duval, The MEDICIS code, a versatile tool for MCCI modelling, International Congress on Advances in Nuclear Power Plants, Seoul, Korea, May 15-19, 2005, Paper 5416.
- [7] R.O. Gauntt, J.E. Cash, R.K. Cole, C.M. Erickson, L.L. Humphries, S.B. Rodriguez, M.F. Young, MELCOR Computer Code Manuals, Sandia National Laboratories, NUREG/CR 6119, SAND2005-5713, 2005.
- [8] D.R. Bradley, D.R. Gardner, J.E. Brockmann, R.O. Griffith, CORCON-MOD3: An Integrated Computer Model for Analysis of Molten Core-Concrete Interactions, Sandia National Laboratories, NUREG/CR-5843, SAND92-0167, 1993.
- [9] B. Spindler, B. Tourniaire, J.M. Seiler, Simulation of MCCI with the TOLBIAC-ICB code based on the phase segregation model, Nuclear Engineering and Design, 236 (2006), 2264-2270.
- [10] J.J. Foit et al., The WECHSL-Mod3 Code: A Computer Program for the Interaction of a Core Melt with Concrete Including the Long Term Behavior. FZKA 5416 (1995).
- [11] J.J. Foit, Modeling oxidic molten core-concrete interaction in WECHSL, Nuclear Engineering and Design, 170 (1997), 73-79.
- [12] J.J. Foit, A. Miassoedov, Modeling of viscosity and heat transfer of complex oxidic melts in WECHSL, Forschungszentrum Karlsruhe, FZKA 5507 (1995).
- [13] J. Langhans, C. Spengler, H. Druwe, ASTEC V1-Description of WEX3.1 Rev0, Report ASTEC-V1/DOC/01-33, GRS and IRSN.